

Hydrogen in Nanocatalysis

Victor Fung, Guoxiang Hu, Zili Wu, and De-en Jiang*

Cite This: *J. Phys. Chem. Lett.* 2020, 11, 7049–7057

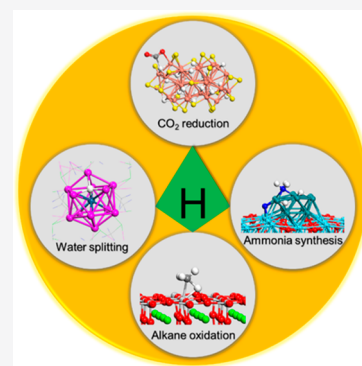
Read Online

ACCESS |

Metrics & More

Article Recommendations

ABSTRACT: Hydrogen is ubiquitous in catalysis. It is involved in many important reactions such as water splitting, N₂ reduction, CO₂ reduction, and alkane activation. In this Perspective, we focus on the hydrogen atom and follow its electron as it interacts with a catalyst or behaves as part of a catalyst from a computational point of view. We present recent examples in both nanocluster and solid catalysts to elucidate the parameters governing the strength of the hydrogen–surface interactions based on site geometry and electronic structure. We further show the interesting behavior of hydride in nanometal and oxides for catalysis. The key take-home messages are: (1) the in-the-middle electronegativity and small size of hydrogen give it great versatility in interacting with active sites on nanoparticles and solid surfaces; (2) the strength of hydrogen binding to an active site on a surface is an important descriptor of the chemical and catalytic properties of the surface; (3) the energetics of the hydrogen binding is closely related to the electronic structure of the catalyst; (4) hydrides in nanoclusters and oxides and on surfaces offer unique reactivity for reduction reactions.



Catalysts are vital in developing a sustainable society, facilitating the generation of green fuels such as hydrogen from water splitting, fertilizer from N₂ fixation, the removal of greenhouse gases by CO₂ reduction, and the conversion of fossil fuels to industrial feedstocks. Key to these catalytic processes is hydrogen, which can take a myriad of roles in the reaction as reactants, products, spectators, promoters, and inhibitors. The variety in function of the hydrogen is also accompanied by a diversity in its chemistry, which can behave as positively charged protons, negatively charged hydrides, or even as pseudometals. One of the origins behind hydrogen's unique properties lies in its moderate electronegativity at 2.2 in the periodic table as measured in the Pauling scale, similar to many catalytically important elements, such as Pt, Ir, Pd, Rh, and Ru. As a result, the charge state of hydrogen can fluctuate significantly depending on its geometric and electronic environment in the material, thereby enabling flexible acid/base and redox chemistry for catalysis. This Perspective aims to

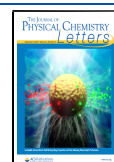
where is the hydrogen located; what is the chemical state of the adsorbed hydrogen; what mechanistic role does hydrogen play in catalysis; and finally, how do we actively tune hydrogen chemistry and reactivity on catalyst surfaces?

Quantum chemistry methods such as density functional theory (DFT) provide a means of addressing these open questions in tandem with experimental studies. Using DFT, the stable adsorption sites and geometries of hydrogen can be obtained, and their electronic properties probed from charge densities to obtain partial atomic charges, or projected orbitals and states. Mechanistic studies on catalysts provide further information on the participation of hydrogen in the reaction and the accompanying reaction energies and barriers. Hydrogen interaction with a catalyst can be used as an important and fast computational probe to evaluate redox and acid/base reactivity of a catalyst. Calculations performed on atomically precise, structurally well-defined nanoclusters can provide clear structure–property relationships with direct experimental corroboration. Calculations performed on model surfaces can provide general trends, helping develop broadly applicable descriptors^{1,2} to predict properties of the diverse surface sites. In both cases, computational chemistry reveals common features regarding hydrogen activity and participation in catalysis.

This Perspective aims to highlight recent efforts in revealing the diversity of hydrogen interactions and their key roles in governing catalysis in both nanoclusters and solid surfaces.

highlight recent efforts in revealing the diversity of hydrogen interactions and their key roles in governing catalysis in both nanoclusters and solid surfaces. The scientific questions we aim to address here regarding hydrogen include the following:

Received: June 9, 2020
Accepted: July 31, 2020
Published: August 3, 2020



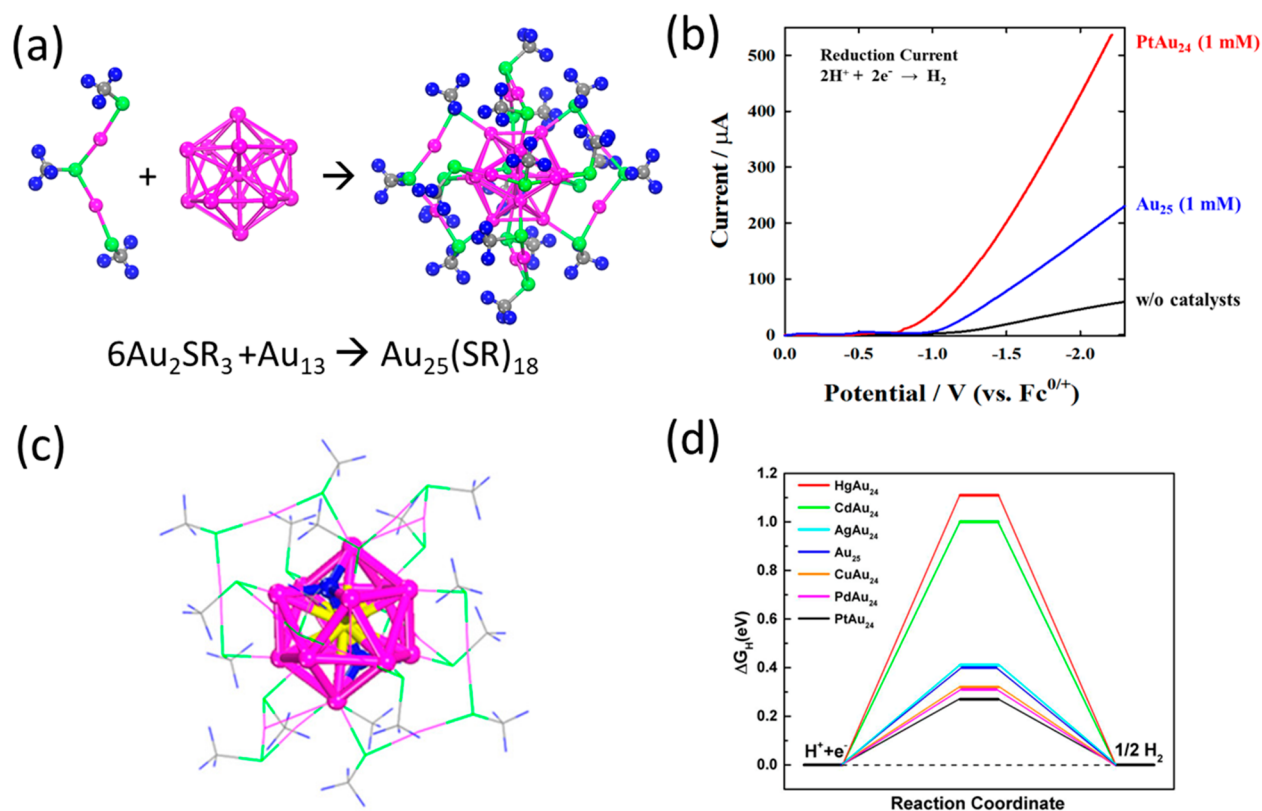


Figure 1. Hydrogen evolution reaction (HER) on undoped and doped $\text{Au}_{25}(\text{SR})_{18}$. (a) Structure of $\text{Au}_{25}(\text{SR})_{18}$ showing the six staple motifs and Au_{13} core. (b) HER performance of pure $\text{Au}_{25}(\text{SR})_{18}$ and Pt-doped $\text{PtAu}_{24}(\text{SR})_{18}$. (c) Hydrogen adsorption geometry in $\text{PtAu}_{24}\text{H}_2(\text{SR})_{18}$. (d) Hydrogen adsorption free energy (ΔG_{H}) of doped $\text{MAu}_{24}(\text{SR})_{18}$. Color code: Au, pink; S, green; C, gray; H, blue; Pt, yellow. [(b) Reprinted with permission from ref 8. Copyright 2017 Nature Publishing Group. (c) Adapted with permission from ref 9. Copyright 2017 American Chemical Society. (d) Reprinted with permission from ref 9. Copyright 2017 American Chemical Society.]

Hydrogen in Nanogold. Investigating the chemistry of hydrogen in atomically precise metal nanoclusters, in particular those of gold, presents a unique opportunity in studying the relationships between hydrogen coordination, charge, and reactivity. Nanogold can be synthesized with wet chemistry techniques and protected with ligands which stabilize into atomically and structurally precise forms.^{3,4} Once crystallized, the structure can be obtained from X-ray or neutron diffraction, providing a useful starting point for computational investigation. Gold is a noble metal and is well-known to interact only weakly with hydrogen, as classically explained by the d-band model.⁵ Consequently, until recently, there had been no structural evidence of hydrogen in nanogold in the literature, unlike the silver and copper nanoparticles in the same coinage group.^{6,7}

Of the stable thiolate-protected solid nanoclusters, $\text{Au}_{25}(\text{SR})_{18}$ is the classic example (Figure 1a), containing an icosahedral Au_{13} core and protected by six $\text{Au}_2(\text{SR})_3$ “staple” ligands, and has been studied for a wide host of catalytic reactions, including the hydrogen evolution reaction (HER).^{8–10} Lee et al. found in a combined theoretical and experimental study that doping of the $\text{Au}_{25}(\text{SR})_{18}$ cluster by Pt to form $\text{Pt}_1\text{Au}_{24}(\text{SR})_{18}$ significantly improves HER activity to beyond that of the state-of-the-art Pt/C catalyst (Figure 1b).⁸ The higher catalytic activity can be explained by a shifting of the originally endothermic hydrogen binding in the Volmer step of HER on $\text{Au}_{25}(\text{SR})_{18}$ of 0.539 eV to a much more favorable, thermodynamically neutral, binding energy of -0.059 eV on the doped $\text{PtAu}_{24}(\text{SR})_{18}$ from DFT calculations

of the proton transfer process from a tetrahydrofuran-solvated proton to an adsorbed hydrogen on the cluster. The hydrogen binding energies have been broadly used as a computational descriptor for HER performance.¹¹

The underlying reasons behind the stronger hydrogen binding on an otherwise noble metal surface were revealed by further DFT studies. We found hydrogen in $\text{Au}_{25}(\text{SR})_{18}$ behaves like a metallic dopant,⁹ rather than the more commonly observed hydride state as a ligand in copper or silver. Metal nanoclusters with high, usually spherical, symmetry can adopt an atom-like electronic structure, or superatom complex, which has been successfully applied to explain the stability of clusters in both bare and ligand-protected forms.¹² Instead of being a negatively charged hydride ligand, the adsorbed hydrogen in $\text{Au}_{25}(\text{SR})_{18}$ has a near-zero charge and contributes its 1s electron to the electron count of the cluster as part of a superatom complex. $\text{Au}_{25}(\text{SR})_{18}^-$ has 8 free electrons which fully occupy the 1S and 1P superatom orbitals to form a closed-shell magic number cluster.^{13,14} When the charge state of $\text{Au}_{25}(\text{SR})_{18}^-$ is changed to $\text{Au}_{25}(\text{SR})_{18}^0$ containing 7 free electrons, the hydrogen adsorption energy is increased from -1.18 to -2.04 eV (in reference to an isolated H atom) because hydrogen in $\text{Au}_{25}(\text{SR})_{18}^0$ completes the stable 8 electron superatom. The same principle can be applied to doping, which changes the free electron count of the cluster.¹³ $\text{PtAu}_{24}(\text{SR})_{18}^0$ has 6 free electrons and can more strongly adsorb two hydrogen (Figure 1c) to complete the superatomic electron count of 8 than $\text{Au}_{25}(\text{SR})_{18}^0$. A visualization of the orbitals showing P-type

HOMO and D-type LUMO provides further evidence of the superatomic electronic structure of the $\text{PtAu}_{24}\text{H}_2(\text{SR})_{18}^0$ cluster.⁹ Besides Pt, other dopants have been screened based on the hydrogen adsorption free energy (ΔG_{H}) as a descriptor for HER (Figure 1d); one can see that when referenced to 1/2 H_2 , hydrogen binding in these clusters is actually unfavorable and there is still plenty of room to tune the chemical property of a gold nanocluster to strengthen the binding and achieve close-to-zero ΔG_{H} . One idea was to explore clusters with weaker coordinating ligands (such as phosphines) and coordinate-unsaturated (*cus*) sites.

Among the atomically precise gold nanoclusters, a phosphine-protected $\text{Au}_{22}(\text{L}_8)_6$ [$\text{L} = 1,8$ -bis-(diphenylphosphino)octane] was synthesized with eight exposed, *cus* gold atoms in the structure which are not bound to any of the phosphines.¹⁵ DFT calculations reveal that hydrogen atoms can be strongly adsorbed on these sites bridging two *cus* gold atoms (Figure 2a).¹⁶ Unlike in the

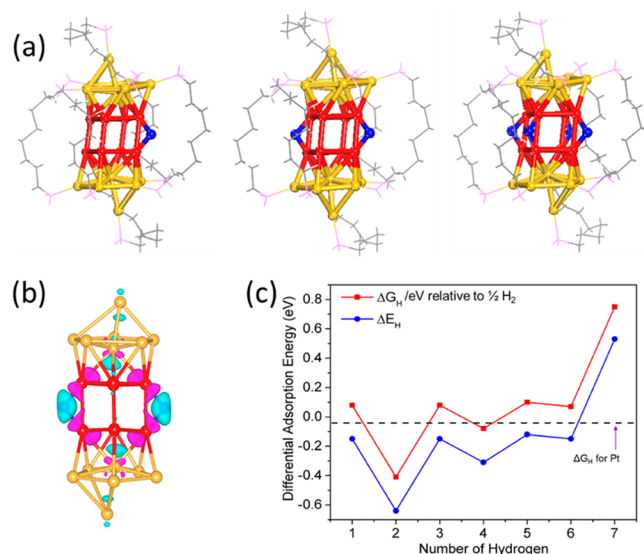


Figure 2. Hydrogen adsorption in $\text{Au}_{22}(\text{L}_8)_6$ [$\text{L} = 1,8$ -bis-(diphenylphosphino)octane]. (a) Hydrogen adsorption geometry of $\text{Au}_{22}(\text{L}_8)_6$ showing one, two, and four hydrogen (in blue) on the undercoordinated gold sites of the cluster (in red). (b) Charge density difference isosurfaces for two hydrogen adsorbed on the cluster, showing electron depletion (pink) from the gold and accumulation in the hydrogen (cyan). (c) Differential hydrogen adsorption energy on $\text{Au}_{22}(\text{L}_8)_6$, with platinum as reference (black dashed line). (Reprinted with permission from ref 16. Copyright 2018 The Royal Society of Chemistry.)

thiolate-protected case where adsorbed H behaves as a metal, hydrogen adsorbed on $\text{Au}_{22}(\text{L}_8)_6$ behaves as a hydride because the more electron-rich nature of the phosphide ligands drives charge transfer from the cluster to the hydrogen (Figure 2b). Up to six hydrogen atoms can be adsorbed on the cluster with favorable energies (Figure 2c). Hence, $\text{Au}_{22}(\text{L}_8)_6$ with eight *cus* gold atoms could be an excellent catalyst for HER, as well as thermal H_2 activation. Further experiments are needed to test this prediction.

Recently, Tsukuda et al. synthesized the first case of a hydrogen-containing $\text{Au}_9\text{H}(\text{PPh}_3)_8^{2+}$, identified using mass spectrometry and NMR spectroscopy.¹⁷ The stability of this cluster was explained by a nearly spherical geometry and a free electron count of 8; hence, hydrogen in this cluster behaves as

a metal, donating its 1s electron to the superatomic electron count. One can therefore conclude that the electronic behavior of hydrogen in a gold nanocluster is very flexible, strongly depending on ligands.

Hydrides in Nanocopper. Copper is known for producing hydrocarbons in CO_2 electroreduction at high overpotentials.¹⁸ In particular, recent studies have shown that high selectivity to hydrocarbons or other C_2 products can be achieved by nanostructured copper with controlled facets or sites.^{19–21} For CO_2 electroreduction at low overpotentials, HER dominates as a competing reaction^{22–24} and needs to be suppressed to obtain higher Faradaic efficiency for CO_2 reduction. Atomically precise copper nanoclusters could help achieve that and bring new insights into CO_2 electroreduction because of their well-defined structure.

Copper nanoclusters tend to contain structural hydrides whose positions can be determined by neutron diffraction.⁷ A prototypical cluster, $\text{Cu}_{32}\text{H}_{20}\text{L}_{12}$ [$\text{L} = \text{S}_2\text{P}(\text{OiPr})_2$],²⁵ was examined for CO_2 electroreduction. After the exploration of various pathways of CO_2 reduction on the model cluster (Figure 3a) by DFT, it was found that the negatively charged hydrides facilitate the formation of HCOOH over CO , thereby dictating the selectivity of the reaction. DFT further predicted that a lattice–hydride mechanism of CO_2 reduction is preferred over the proton-reduction mechanism (Figure 3b). The schematic of the lattice–hydride mechanism for the formation of HCOOH on the $\text{Cu}_{32}\text{H}_{20}\text{L}_{12}$ cluster is shown in Figure 3c: CO_2 adsorbs atop an exposed hydride (left) and then reacts with it to form the formate (top), which reacts with a second lattice hydride to form HCOOH and desorbs (right), leaving two H vacancies which are regenerated via proton reduction (bottom). Both HER and CO formation were found to be kinetically unfavorable from computed reaction barriers. The computational prediction was validated experimentally from electrocatalytic testing showing the selective production of HCOOH over CO and H_2 at low overpotentials (Figure 3d). The above example is the first demonstration of a lattice–hydride mechanism for electrochemical CO_2 reduction in clusters or solid surfaces, which inspired further study of copper–hydride nanoclusters for hydrogenation catalysis.²⁶

Hydrides in Oxides, Nitrides, and Electrides. Hydrides as an anion could also be part of a mixed-anion compound as in oxides, nitrides, and electrides. The ABO_3 perovskite structure can incorporate hydride by the substitution of hydride anions for oxide. For example, $\text{BaTiO}_{3-x}\text{H}_x$ perovskite oxyhydride with $x \leq 0.60$ was prepared,²⁷ which found many applications in catalysis such as ammonia synthesis.²⁸ Although the detailed mechanism is still unclear, it is speculated that the labile hydrides provide a spillover pathway for H_2 .

Electrides are ionic materials where the anion is partially composed of solvated electrons. Hosono and others have found ruthenium, a classic ammonia synthesis catalyst, supported on various electrides such as C12A7 ($12\text{CaO} \cdot 7\text{Al}_2\text{O}_3$ or $\text{Ca}_{12}\text{Al}_{14}\text{O}_{33}$) and Ca_2N had much better catalytic activities than the pure ruthenium particles.^{29–31} Under reaction conditions, the electride Ca_2N was transformed into the hydride Ca_2NH which maintained the high catalytic activity. A lowered N_2 activation barrier was observed and attributed to the electronic donation of the hydride to the ruthenium particles.

A new oxynitride hydride, $\text{BaCeO}_{3-x}\text{N}_y\text{H}_z$, was synthesized from a CeO_2 and $\text{Ba}(\text{NH}_2)_2$ precursor (Figure 4a).³² The rate-limiting step of ammonia synthesis is no longer N_2

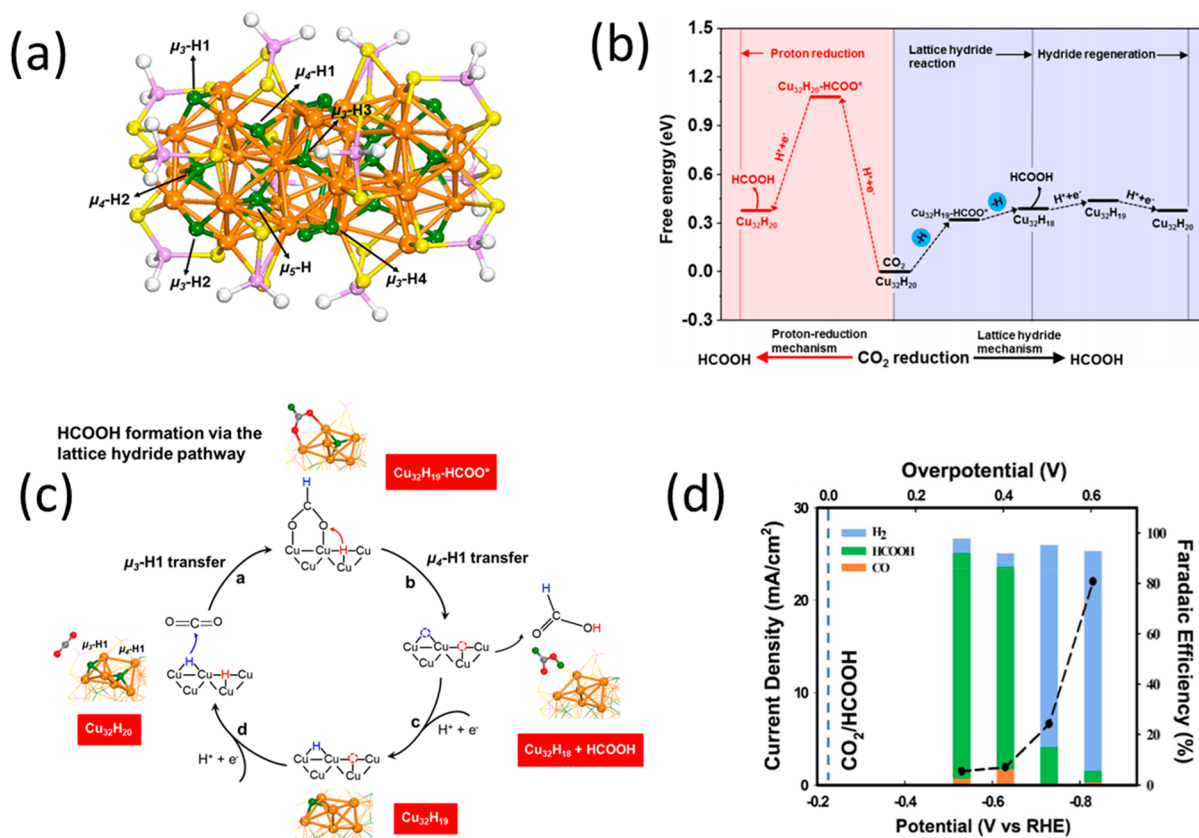


Figure 3. Electroreduction of CO_2 on the $\text{Cu}_{32}\text{H}_{20}\text{L}_{12}$ cluster. (a) Structure of the $\text{Cu}_{32}\text{H}_{20}\text{L}_{12}$ cluster ($\text{L} = \text{S}_2\text{PH}_2$ in the DFT model). (b) Free-energy profile for the formation of HCOOH from CO_2 on $\text{Cu}_{32}\text{H}_{20}\text{L}_{12}$: lattice-hydride vs proton-reduction mechanism. (c) Schematic of the lattice-hydride mechanism for the formation of HCOOH. (d) Experimental product distribution and Faradaic efficiency for H_2 , HCOOH, and CO produced at different potentials. (Reprinted with permission from ref 25. Copyright 2017 American Chemical Society.)

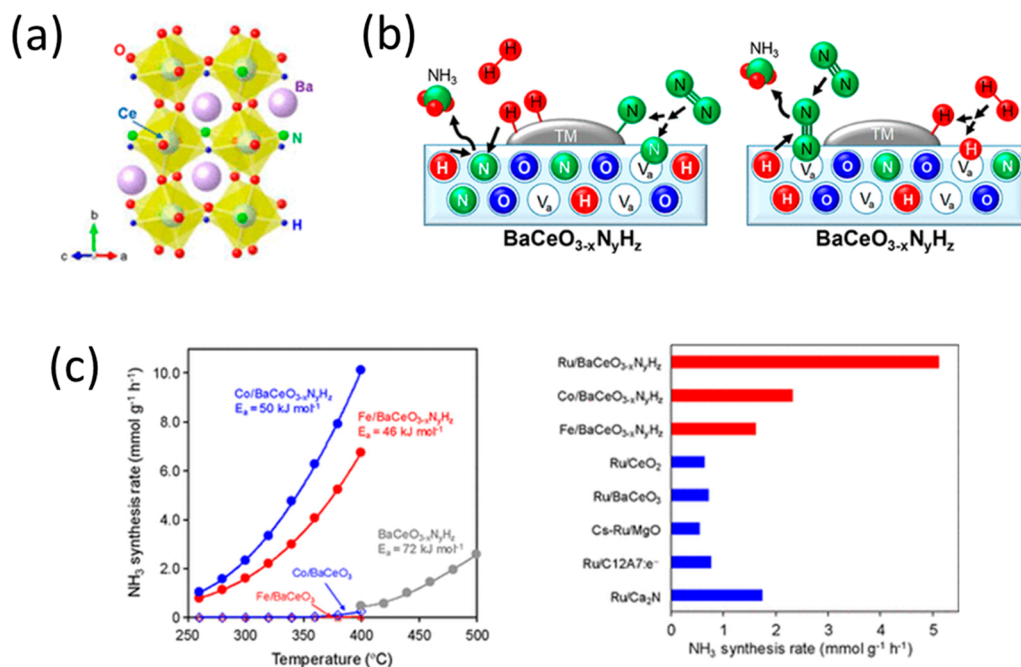


Figure 4. Ammonia synthesis on perovskite oxynitride hydride catalysts. (a) Crystal structure of $\text{BaCeO}_{3-x}\text{N}_y\text{H}_z$. (b) Proposed Mars-van-Krevelen reaction mechanisms for ammonia synthesis on the lattice nitride sites. (c) Ammonia synthesis performance with different supported metals compared with other catalysts. (Reprinted with permission from ref 32. Copyright 2019 American Chemical Society.)

dissociation, but N–H formation. A mechanism was proposed (Figure 4b) in which lattice hydrogen forms N–H bonds with

either the lattice nitrogen or dissociated nitrogen from the reactants. The new catalyst outperforms conventional

ruthenium as well as electroneutral-supported ruthenium for ammonia synthesis (Figure 4c). The presence of lattice hydrides shared by these materials could be the key for enhanced catalytic performance. Mechanistic understanding of the role of hydrides is in its infancy for these systems, and further experimental and theoretical investigations are urgently needed.³³

Hydrogen Adsorption and C–H Activation on Oxides. The examples above focus on the reduction reaction and hydrogen as a structural element of the catalysts. Next we focus on oxidation reactions, especially C–H activation and the role of hydrogen on surfaces.

Metal oxides are well-established catalysts for alkane activation and conversion.^{34,35} Key to the ability of metal oxides for activating the C–H bond in alkanes is the activity of the lattice oxygen. Regardless of the final product in alkane conversion, the C–H bond must first be broken to form an adsorbed alkyl and hydrogen. On the majority of metal oxides under oxidative conditions, hydrogen preferentially adsorbs on the lattice oxygen to form hydroxyls with a positively charged hydrogen. The bonding of hydrogen with oxygen here is characterized as a polar covalent one, with a significant degree of charge transfer from hydrogen to oxygen as directed by their relative electronegativities. Alkane C–H activation follows two general mechanisms, a heterolytic C–H pathway involving the insertion of an M–O bond and a homolytic C–H pathway involving hydrogen-abstraction by an oxygen species in metal oxides (Figure 5a). A large number of computational studies on oxides in recent years have investigated and concluded the favorability for the homolytic C–H activation pathway in a large number of redox-active oxides.^{36,37} In this pathway, oxygen is the only species responsible for bond breaking in the transition state, and its chemistry directly determines the energy barrier for activation.

Further improving our ability to efficiently predict hydrogen adsorption energy from electronic structure or geometric information will dramatically improve the feasibility of the high-throughput screening of catalytic materials.

Hydrogen adsorption energy (HAE) has turned out to be an excellent descriptor for homolytic C–H activation (Figure 5b). On transition metal oxides, doped transition metal oxides, and perovskites, we found a strong linear correlation between hydrogen adsorption energy (HAE) and the C–H activation energy for ethane and methane, where a stronger HAE correlated with lower C–H activation barriers.^{38–40} Iglesia et al. found similar correlations between HAE and the C–H activation energies for various C₁–C₃ alkanes and oxygenates in polyoxometalate systems in combined theoretical and experimental studies.^{41,42} Norskov et al. found the correlation exists for a broad number of systems, including oxides but also zeolites, metal-organic frameworks, as well as oxygen species on 2D materials, metals, and metal clusters.⁴³ The reason for this relationship can be explained according to the Bronsted–Evans–Polanyi principle, where the relative activation energies are proportional to the reaction energies. In this case, the reaction energy in homolytic C–H activation is the difference

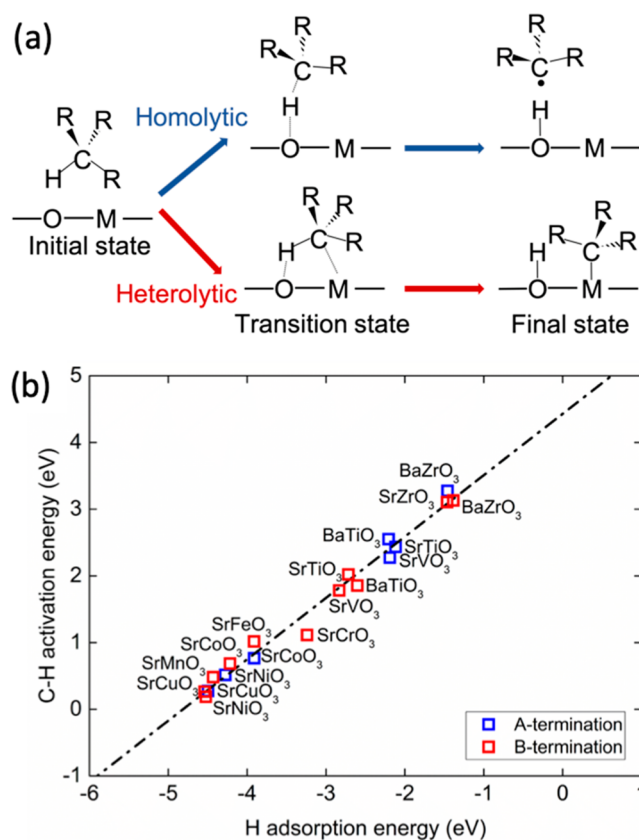


Figure 5. Hydrogen-adsorption energy as a C–H activation descriptor. (a) Two primary mechanisms for C–H activation on metal oxides. (b) Correlation between homolytic C–H activation energy of CH₄ with hydrogen adsorption energy on various perovskite (001) A and B terminations. [(b) Reprinted with permission from ref 40. Copyright 2018 The Royal Society of Chemistry.]

in energy between a CH₄ (as an example) in the gas phase and a CH₃ in the gas phase with a OH group on the surface. For the same reactant on different surfaces, the difference in reactant energy is therefore the difference in hydrogen adsorption energy to form the O–H. The HAE descriptor can be expanded to different reactants by including the bond dissociation energy difference of the reactants in the same theoretical framework, as well as additional term(s) describing the radical–surface interaction.⁴¹

Correlation of Oxygen-Vacancy Formation and Oxygen Coordination to Hydrogen Adsorption. Hydrogen adsorption on an oxide surface can be viewed as a measure of the reducibility of the surface and hence can be linked to other redox descriptors such as oxygen-vacancy formation energy (OVFE), valence-band maximum, conduction-band minimum, etc. For example, Janik et al. demonstrated that OVFE is an effective descriptor for homolytic C–H activation on doped CeO₂ and other metal oxides.^{44,45} A corresponding linear correlation between HAE and OVFE was subsequently found in many examples.^{38,43} A stronger HAE was found to correlate to a lower OVFE. As both quantities can be characterized by a reduction of the surface (one-electron reduction for hydrogen adsorption and two-electron reduction for the O-vacancy formation), they can be used to relate to the reducibility of the surface.

HAE can also be correlated to a geometric descriptor based on the coordination number of surface oxygen.³⁸ The higher

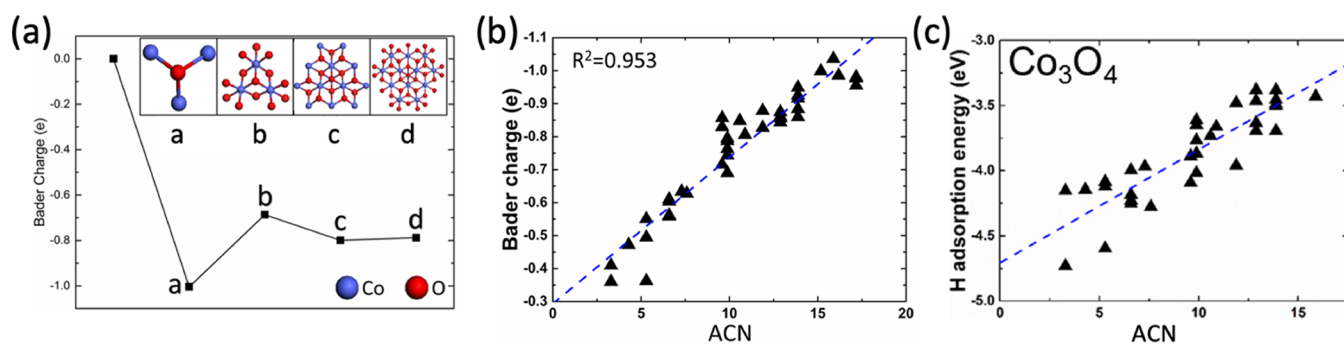


Figure 6. Geometric descriptor relating the coordination environment of a surface oxygen to its charge and hydrogen adsorption energy, using Co_3O_4 as an example. (a) Variation and convergence of Bader charge on an oxygen atom as its coordination shells are progressively added as in bulk Co_3O_4 . (b) Correlation between Bader charge and the adjusted coordination number (ACN) of oxygen sites on Co_3O_4 surfaces. (c) Correlation between hydrogen adsorption energy and ACN of oxygen sites on Co_3O_4 surfaces. [Adapted with permission from ref 38. Copyright 2017 American Chemical Society.]

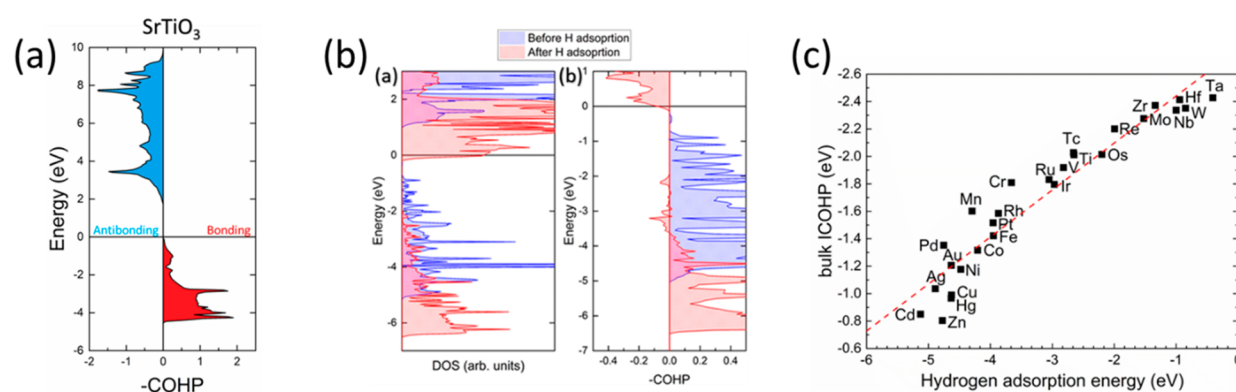


Figure 7. Bulk descriptor relating the strength of the M–O bond to hydrogen adsorption on a specific surface. (a) The crystal-orbital Hamiltonian population (COHP) versus energy for SrTiO_3 showing bonding (red) and antibonding (blue) interactions. (b) Density of states and COHP of the Ti–O bond before and after hydrogen adsorption on $\text{SrTiO}_3(100)$. (c) Correlation between integrated COHP and hydrogen adsorption energy on the lattice oxygen of $\text{SrMO}_3(100)$ for M being transition metals. [Adapted with permission from ref 49. Copyright 2018 American Chemical Society.]

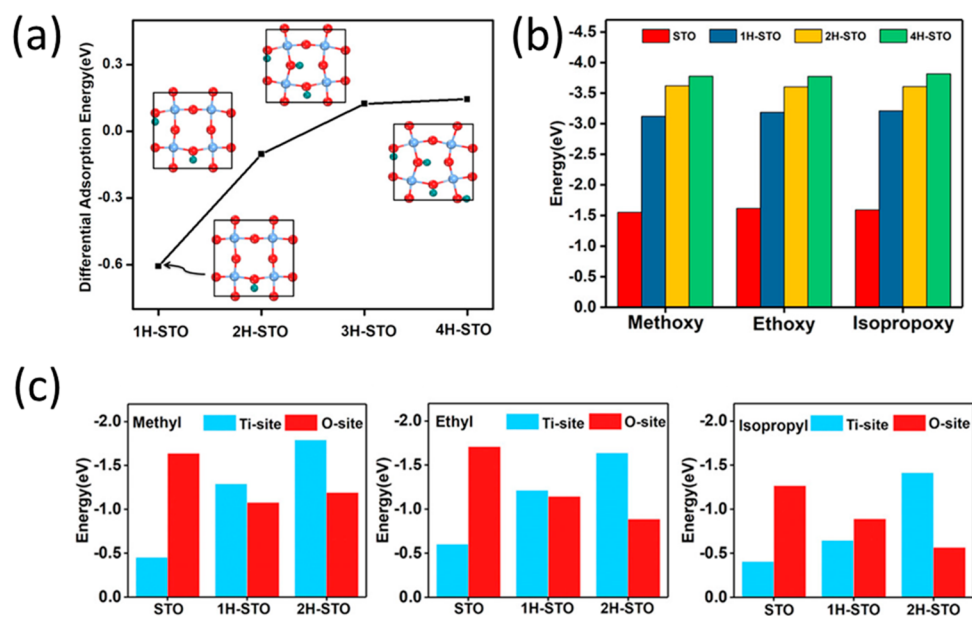


Figure 8. Effect of surface metallization on chemisorption energies on SrTiO_3 . (a) Hydrogen adsorption energy and geometry. (b) Adsorption energy of oxygenates on the pristine and H-functionalized surface. (c) Adsorption energy of alkyl radicals on the pristine and H-functionalized surface. [Reprinted with permission from ref 54. Copyright 2019 American Chemical Society.]

the coordination number on an oxygen, the more negatively charged the oxygen atom. Meanwhile, the higher the coordination number of the metal atoms in the first coordination shell of the oxygen atom, the less negatively charged the central oxygen (Figure 6a). This compensating effect of the first and second coordination shells of an oxygen atom led to the development of the adjusted coordination number or ACN which can be used to predict the partial atomic charge and correspondingly the HAE on a surface oxygen (Figure 6b). Further improvement to accuracy of ACN was demonstrated by Wang et al. including the bond length.⁴⁶ ACN and its other iterations can be used to quickly predict adsorption and C–H activation energy for the different surfaces and terminations of a given oxide (Figure 6c).

Where Is the Electron after Hydrogen Adsorption? The reduction of a metal oxide (MO) surface after hydrogen adsorption can be further understood by following the electron associated with hydrogen adsorption, especially its impact on the M–O bond. This can be done by calculating the crystal orbital Hamilton populations (COHPs) of the metal and oxygen interactions.^{47,48} The COHP is obtained by partitioning the band structure into bonding and antibonding contributions, where a negative (positive) sign denotes bonding (antibonding). Integrating the COHP provides an indicator (ICOHP) of the bond strength: a more negative ICOHP suggests a stronger bond. The covalent nature of the transition metal M–O bond arises from the overlap of the oxygen 2p orbitals and the metal d orbitals, leading to the formation of bonding and antibonding states (Figure 7a).^{49,50} On model SrMO₃ perovskites, as the d-electron count increases in the metal, there is a corresponding filling of the antibonding states of the M–O bond, thereby weakening it. Similarly, a reduction of the surface by a hydrogen will fill the antibonding states of the M–O bond (Figure 7b). This reduction constitutes an energetic “penalty” from weakening the M–O bond, which is balanced out by the O–H covalent bonding energy. A general rule can be observed: the stronger the M–O bond, the greater the extent of weakening of that bond from reduction by hydrogen. A consequence of this relation is that the M–O bond strength (obtained using the ICOHP of the M–O bond) can therefore correlate to the HAE in a linear scaling relationship (Figure 7c). The impact of the electron transfer to the antibonding states on surface chemistry was also observed in non-oxide materials such as MoS₂.⁵¹

Electron donation to the M–O antibonding states (at the conduction band minimum) from hydrogen adsorption can induce surface metallization in oxides such as SrTiO₃,^{52,53} which in turn impacts the surface chemistry.⁵⁴ For example, adsorption of one or more hydrogen on the SrTiO₃(100) surface (Figure 8a) results in an insulator-to-metal transition where the conduction band becomes partially occupied. By probing the interaction of common oxygenate radicals such as methoxy, ethoxy, and isopropoxy on the lattice Ti, the adsorption was found to become considerably stronger from around –1.5 eV up to –3.8 eV at high H coverages (Figure 8b). The effect was even more dramatic for alkyl radicals, which adsorb on lattice oxygen for the pristine surface but undergo a change in site preference to lattice Ti accompanied by a similar increase in adsorption strength upon metallization by hydrogen (Figure 8c). These results provide a first look into the impact of hydrogen-induced metallization on chemisorption with important implications for catalysis.

H₂ Activation and Kinetically Stabilized Hydrides on Oxides. The discussion above has mainly focused on the energetics of atomic H adsorption on oxides where the usually preferred site is the surface lattice oxygen, leading to a surface hydroxyl formation after adsorption. Recently, some cases of surface hydride formation on the surface metal-ion sites have been reported. To compare the different sites for atomic H adsorption and to consider especially the kinetic factor, H₂ activation on the most commonly examined surfaces of different TiO₂ polymorphs, including rutile TiO₂(110), anatase TiO₂(101), and brookite TiO₂(210), was examined by DFT.⁵⁵ Both the heterolytic pathway (leading to a hydride and a hydroxyl) and the homolytic pathway (leading to two hydroxyls) were considered. It was found that for all three surfaces, the heterolytic pathway is kinetically more favorable, even though the homolytic pathway is thermodynamically more favorable. Interestingly, it was that after the heterolytic cleavage, the transfer of H from Ti to O has a high barrier (>1.5 eV) on anatase TiO₂(101) and brookite TiO₂(210), indicating that hydrides on anatase TiO₂(101) and brookite TiO₂(210) can be kinetically stabilized. This finding is consistent with a recent experimental report of the H–Ti species on anatase TiO₂,⁵⁶ which may facilitate surface chemistry on TiO₂.

Concluding Remarks. The above examples seek to highlight the central role of hydrogen in nanocatalysis. In particular, the charge state of the hydrogen (and the corresponding direction of electron flow) and its bonding strength determines the activity of the catalysts. In thiolate-protected gold nanoclusters, hydrogen behaves as a metal, thereby enabling the superatomic electronic structure during hydrogen evolution reaction. The coordinate-unsaturated sites in gold nanoclusters provide the most promising energetics for hydrogen evolution and H₂ activation. Negatively charged hydrides in copper nanoclusters yielded unique selectivity in electroreduction of CO₂ following a lattice–hydride mechanism.

The hydrogen adsorption energy is an important descriptor for C–H activation and alkane oxidation on transition-metal oxides and ABO₃ perovskites, and the adsorption strength can be tuned by doping, surface coordination, and bulk composition. From the computational perspective, hydrogen adsorption is a simple but powerful descriptor which can probe the chemistry of clusters and solids. The judicious use of this information can also further predict the catalytic performance of a host of oxidation and reduction reactions.

As new materials continue to be discovered and investigated in catalysis, the energy and charge transfer from hydrogen adsorption is expected to continue to be an important descriptor in the computational chemistry repertoire. Further improving our ability to efficiently predict hydrogen adsorption energy from electronic structure or geometric information will dramatically improve the feasibility of the high-throughput screening of catalytic materials. In addition, finding the (most) stable adsorption sites of hydrogen in complex materials is a complementary problem which needs to be solved, and applying machine learning techniques has great promise in this regard.^{57,58} From the materials perspective, hydrides in solids such as electrides and oxyhydrides, and those residing at interfaces of supported particles and 2D materials, have exciting unexplored potential for catalysis. There is still much new chemistry and many applications to develop from hydrogen either in the bulk structure or on surfaces of nanocatalysts by using computational chemistry.

■ AUTHOR INFORMATION

Corresponding Author

De-en Jiang – Department of Chemistry, University of California, Riverside, California 92521, United States; orcid.org/0000-0001-5167-0731; Email: djiang@ucr.edu

Authors

Victor Fung – Department of Chemistry, University of California, Riverside, California 92521, United States; Center for Nanophase Materials Sciences, Oak Ridge National Laboratory, Oak Ridge, Tennessee 37831, United States; orcid.org/0000-0002-3347-6983

Guoxiang Hu – Department of Chemistry, University of California, Riverside, California 92521, United States; Center for Nanophase Materials Sciences, Oak Ridge National Laboratory, Oak Ridge, Tennessee 37831, United States; orcid.org/0000-0003-2942-8564

Zili Wu – Center for Nanophase Materials Sciences and Chemical Sciences Division, Oak Ridge National Laboratory, Oak Ridge, Tennessee 37831, United States; orcid.org/0000-0002-4468-3240

Complete contact information is available at: <https://pubs.acs.org/10.1021/acs.jpcllett.0c01783>

Notes

The authors declare no competing financial interest.

Biographies

Victor Fung is a Eugene P. Wigner Fellow at Oak Ridge National Laboratory (ORNL). He obtained his B.A. in Chemistry from Cornell University and his Ph.D. in Chemistry from the University of California, Riverside (UCR). His research involves the study of surfaces and catalytic properties from first principles.

Guoxiang Hu is a Postdoctoral Research Associate at ORNL. She received her B.S. from the University of Science and Technology of China and Ph.D. in chemistry from UCR. Her research focuses on using computational chemistry to study functional materials for energy sustainability.

Zili Wu is a senior research staff at ORNL. He obtained his B.S. in Environmental Chemistry from Wuhan University and PhD in Physical Chemistry from Dalian Institute of Physical Chemistry. His research interest focuses on fundamental heterogeneous catalysis and photocatalysis as well as *in situ* and *operando* methods including optical and neutron spectroscopy.

De-en Jiang is a professor of chemistry at UCR. He received his B.S. and M.S. from Peking University and Ph.D. from UCLA. He was a staff scientist at ORNL before joining UCR in 2014. His research focuses on computational materials chemistry and nanoscience for energy and the environment.

■ ACKNOWLEDGMENTS

This work was sponsored by the U.S. Department of Energy, Office of Science, Office of Basic Energy Sciences, Chemical Sciences, Geosciences, and Biosciences Division, Catalysis Science Program. This research used resources of the National Energy Research Scientific Computing Center, a DOE Office of Science User Facility supported by the Office of Science of the U.S. Department of Energy under contract no. DE-AC02-05CH11231.

■ REFERENCES

- (1) Nørskov, J. K.; Abild-Pedersen, F.; Studt, F.; Bligaard, T. Density Functional Theory in Surface Chemistry and Catalysis. *Proc. Natl. Acad. Sci. U. S. A.* **2011**, *108*, 937–943.
- (2) Zhao, Z.-J.; Liu, S.; Zha, S.; Cheng, D.; Studt, F.; Henkelman, G.; Gong, J. Theory-guided Design of Catalytic Materials Using Scaling Relationships and Reactivity Descriptors. *Nat. Rev. Mater.* **2019**, *4*, 792–804.
- (3) Jin, R.; Zeng, C.; Zhou, M.; Chen, Y. Atomically Precise Colloidal Metal Nanoclusters and Nanoparticles: Fundamentals and Opportunities. *Chem. Rev.* **2016**, *116*, 10346–10413.
- (4) Tang, Q.; Jiang, D.-e. Computational Insight into the Covalent Organic-Inorganic Interface. *Chem. Mater.* **2016**, *28*, 5976–5988.
- (5) Hammer, B.; Nørskov, J. Why Gold is the Noblest of All the Metals. *Nature* **1995**, *376*, 238–240.
- (6) Bootharaju, M. S.; Dey, R.; Gevers, L. E.; Hedhili, M. N.; Basset, J.-M.; Bakr, O. M. A New Class of Atomically Precise, Hydride-Rich Silver Nanoclusters Co-Protected by Phosphines. *J. Am. Chem. Soc.* **2016**, *138*, 13770–13773.
- (7) Dhayal, R. S.; van Zyl, W. E.; Liu, C. W. Polyhydrido Copper Clusters: Synthetic Advances, Structural Diversity, and Nanocluster-to-Nanoparticle Conversion. *Acc. Chem. Res.* **2016**, *49*, 86–95.
- (8) Kwak, K.; Choi, W.; Tang, Q.; Kim, M.; Lee, Y.; Jiang, D.-e.; Lee, D. A Molecule-like PtAu₂₄(SC₆H₁₃)₁₈ Nanocluster as an Electro-catalyst for Hydrogen Production. *Nat. Commun.* **2017**, *8*, 14723.
- (9) Hu, G.; Tang, Q.; Lee, D.; Wu, Z.; Jiang, D.-e. Metallic Hydrogen in Atomically Precise Gold Nanoclusters. *Chem. Mater.* **2017**, *29*, 4840–4847.
- (10) Kang, X.; Chong, H.; Zhu, M. Au₂₅(SR)₁₈: the Captain of the Great Nanocluster Ship. *Nanoscale* **2018**, *10*, 10758–10834.
- (11) Greeley, J.; Jaramillo, T. F.; Bonde, J.; Chorkendorff, I.; Nørskov, J. K. Computational High-throughput Screening of Electrocatalytic Materials for Hydrogen Evolution. *Nat. Mater.* **2006**, *5*, 909–913.
- (12) Walter, M.; Akola, J.; Lopez-Acevedo, O.; Jadzinsky, P. D.; Calero, G.; Ackerson, C. J.; Whetten, R. L.; Gronbeck, H.; Hakkinen, H. A Unified View of Ligand-protected Gold Clusters as Superatom Complexes. *Proc. Natl. Acad. Sci. U. S. A.* **2008**, *105*, 9157–62.
- (13) Jiang, D.-e.; Dai, S. From Superatomic Au₂₅(SR)₁₈[−] to Superatomic M@Au₂₄(SR)₁₈^q Core-Shell Clusters. *Inorg. Chem.* **2009**, *48*, 2720–2722.
- (14) Akola, J.; Walter, M.; Whetten, R. L.; Häkkinen, H.; Grönbeck, H. On the Structure of Thiolate-Protected Au₂₅. *J. Am. Chem. Soc.* **2008**, *130*, 3756–3757.
- (15) Chen, J.; Zhang, Q.-F.; Bonaccorso, T. A.; Williard, P. G.; Wang, L.-S. Controlling Gold Nanoclusters by Diphosphine Ligands. *J. Am. Chem. Soc.* **2014**, *136*, 92–95.
- (16) Hu, G.; Wu, Z.; Jiang, D.-e. Stronger-than-Pt Hydrogen Adsorption in a Au₂₂ Nanocluster for the Hydrogen Evolution Reaction. *J. Mater. Chem. A* **2018**, *6*, 7532–7537.
- (17) Takano, S.; Hirai, H.; Muramatsu, S.; Tsukuda, T. Hydride-Doped Gold Superatom (Au₉H)²⁺: Synthesis, Structure, and Transformation. *J. Am. Chem. Soc.* **2018**, *140*, 8380–8383.
- (18) Hori, Y.; Murata, A.; Takahashi, R. Formation of Hydrocarbons in the Electrochemical Reduction of Carbon Dioxide at a Copper Electrode in Aqueous Solution. *J. Chem. Soc., Faraday Trans. 1* **1989**, *85*, 2309–2326.
- (19) Wang, Y.; Wang, Z.; Dinh, C.-T.; Li, J.; Ozden, A.; Golam Kibria, M.; Seifitokaldani, A.; Tan, C.-S.; Gabardo, C. M.; Luo, M.; et al. Catalyst Synthesis under CO₂ Electroreduction Favours Faceting and Promotes Renewable Fuels Electrosynthesis. *Nat. Catal.* **2020**, *3*, 98–106.
- (20) Luc, W.; Fu, X.; Shi, J.; Lv, J.-J.; Jouny, M.; Ko, B. H.; Xu, Y.; Tu, Q.; Hu, X.; Wu, J.; et al. Two-dimensional Copper Nanosheets for Electrochemical Reduction of Carbon Monoxide to Acetate. *Nat. Catal.* **2019**, *2*, 423–430.
- (21) Zhong, M.; Tran, K.; Min, Y.; Wang, C.; Wang, Z.; Dinh, C.-T.; De Luna, P.; Yu, Z.; Rasouli, A. S.; Brodersen, P.; et al. Accelerated

Discovery of CO₂ Electrocatalysts Using Active Machine Learning. *Nature* **2020**, *581*, 178–183.

(22) Lu, Q.; Rosen, J.; Zhou, Y.; Hutchings, G. S.; Kimmel, Y. C.; Chen, J. G.; Jiao, F. A Selective and Efficient Electrocatalyst for Carbon Dioxide Reduction. *Nat. Commun.* **2014**, *5*, 3242.

(23) Li, M.; Zhang, Y.; Li, X.; Wang, Y.; Dong, F.; Ye, L.; Yu, S.; Huang, H. Nature-Derived Approach to Oxygen and Chlorine Dual-Vacancies for Efficient Photocatalysis and Photoelectrochemistry. *ACS Sustainable Chem. Eng.* **2018**, *6*, 2395–2406.

(24) Huang, J.-F.; Wu, Y.-C. Tunable Ag Micromorphologies Show High Activities for Electrochemical H₂ Evolution and CO₂ Electrochemical Reduction. *ACS Sustainable Chem. Eng.* **2019**, *7*, 6352–6359.

(25) Tang, Q.; Lee, Y.; Li, D.-Y.; Choi, W.; Liu, C. W.; Lee, D.; Jiang, D.-e. Lattice-Hydride Mechanism in Electrocatalytic CO₂ Reduction by Structurally Precise Copper-Hydride Nanoclusters. *J. Am. Chem. Soc.* **2017**, *139*, 9728–9736.

(26) Sun, C.; Mammen, N.; Kaappa, S.; Yuan, P.; Deng, G.; Zhao, C.; Yan, J.; Malola, S.; Honkala, K.; Häkkinen, H.; et al. Atomically Precise, Thiolated Copper-Hydride Nanoclusters as Single-Site Hydrogenation Catalysts for Ketones in Mild Conditions. *ACS Nano* **2019**, *13*, 5975–5986.

(27) Kobayashi, Y.; Hernandez, O. J.; Sakaguchi, T.; Yajima, T.; Roisnel, T.; Tsujimoto, Y.; Morita, M.; Noda, Y.; Mogami, Y.; Kitada, A.; et al. An Oxyhydride of BaTiO₃ Exhibiting Hydride Exchange and Electronic Conductivity. *Nat. Mater.* **2012**, *11*, 507–511.

(28) Tang, Y.; Kobayashi, Y.; Masuda, N.; Uchida, Y.; Okamoto, H.; Kageyama, T.; Hosokawa, S.; Loyer, F.; Mitsuhashi, K.; Yamanaka, K.; et al. Metal-Dependent Support Effects of Oxyhydride-Supported Ru, Fe, Co Catalysts for Ammonia Synthesis. *Adv. Energy Mater.* **2018**, *8*, 1801772.

(29) Hara, M.; Kitano, M.; Hosono, H. Ru-Loaded C12A7:e⁻ Electride as a Catalyst for Ammonia Synthesis. *ACS Catal.* **2017**, *7*, 2313–2324.

(30) Kitano, M.; Inoue, Y.; Ishikawa, H.; Yamagata, K.; Nakao, T.; Tada, T.; Matsuishi, S.; Yokoyama, T.; Hara, M.; Hosono, H. Essential Role of Hydride ion in Ruthenium-based Ammonia Synthesis Catalysts. *Chem. Sci.* **2016**, *7*, 4036–4043.

(31) Kammert, J.; Moon, J.; Cheng, Y.; Daemen, L.; Irlé, S.; Fung, V.; Liu, J.; Page, K.; Ma, X.; Phaneuf, V.; et al. Nature of Reactive Hydrogen for Ammonia Synthesis over a Ru/C12A7 Electride Catalyst. *J. Am. Chem. Soc.* **2020**, *142*, 7655–7667.

(32) Kitano, M.; Kujirai, J.; Ogasawara, K.; Matsuishi, S.; Tada, T.; Abe, H.; Niwa, Y.; Hosono, H. Low-Temperature Synthesis of Perovskite Oxynitride-Hydrides as Ammonia Synthesis Catalysts. *J. Am. Chem. Soc.* **2019**, *141*, 20344–20353.

(33) Esposito, D. The Importance of Being Hydride. *Nat. Catal.* **2018**, *1*, 897–897.

(34) Sattler, J. J. H. B.; Ruiz-Martinez, J.; Santillan-Jimenez, E.; Weckhuysen, B. M. Catalytic Dehydrogenation of Light Alkanes on Metals and Metal Oxides. *Chem. Rev.* **2014**, *114*, 10613–10653.

(35) Coperet, C. C-H Bond Activation and Organometallic Intermediates on Isolated Metal Centers on Oxide Surfaces. *Chem. Rev.* **2010**, *110*, 656–680.

(36) Latimer, A. A.; Aljama, H.; Kakekhani, A.; Yoo, J. S.; Kulkarni, A.; Tsai, C.; Garcia-Melchor, M.; Abild-Pedersen, F.; Nørskov, J. K. Mechanistic Insights Into Heterogeneous Methane Activation. *Phys. Chem. Chem. Phys.* **2017**, *19*, 3575–3581.

(37) Rozanska, X.; Fortrie, R.; Sauer, J. Size-Dependent Catalytic Activity of Supported Vanadium Oxide Species: Oxidative Dehydrogenation of Propane. *J. Am. Chem. Soc.* **2014**, *136*, 7751–7761.

(38) Fung, V.; Tao, F. F.; Jiang, D. E. General Structure-Reactivity Relationship for Oxygen on Transition-Metal Oxides. *J. Phys. Chem. Lett.* **2017**, *8*, 2206–2211.

(39) Fung, V.; Tao, F. F.; Jiang, D.-e. Trends of Alkane Activation on Doped Cobalt (II, III) Oxide from First Principles. *ChemCatChem* **2018**, *10*, 244–249.

(40) Fung, V.; Polo-Garzon, F.; Wu, Z.; Jiang, D.-e. Exploring Perovskites for Methane Activation from First Principles. *Catal. Sci. Technol.* **2018**, *8*, 702–709.

(41) Deshlahra, P.; Iglesia, E. Reactivity and Selectivity Descriptors for the Activation of C-H Bonds in Hydrocarbons and Oxygenates on Metal Oxides. *J. Phys. Chem. C* **2016**, *120*, 16741–16760.

(42) Deshlahra, P.; Iglesia, E. Toward More Complete Descriptors of Reactivity in Catalysis by Solid Acids. *ACS Catal.* **2016**, *6*, 5386–5392.

(43) Latimer, A. A.; Kulkarni, A. R.; Aljama, H.; Montoya, J. H.; Yoo, J. S.; Tsai, C.; Abild-Pedersen, F.; Studt, F.; Nørskov, J. K. Understanding Trends in CH Bond Activation in Heterogeneous Catalysis. *Nat. Mater.* **2017**, *16*, 225–229.

(44) Kumar, G.; Lau, S. L. J.; Krcha, M. D.; Janik, M. J. Correlation of Methane Activation and Oxide Catalyst Reducibility and its Implications for Oxidative Coupling. *ACS Catal.* **2016**, *6*, 1812–1821.

(45) Krcha, M. D.; Mayernick, A. D.; Janik, M. J. Periodic Trends of Oxygen Vacancy Formation and C-H Bond Activation Over Transition Metal-Doped CeO₂ (111) Surfaces. *J. Catal.* **2012**, *293*, 103–115.

(46) Zhou, C.; Zhang, B.; Hu, P.; Wang, H. An Effective Structural Descriptor to Quantify the Reactivity of Lattice Oxygen in CeO₂ Subnano-clusters. *Phys. Chem. Chem. Phys.* **2020**, *22*, 1721–1726.

(47) Dronskowski, R.; Bloechl, P. E. Crystal Orbital Hamilton Populations (COHP): Energy-Resolved Visualization of Chemical Bonding in Solids Based on Density-Functional Calculations. *J. Phys. Chem.* **1993**, *97*, 8617–8624.

(48) Glassey, W. V.; Hoffmann, R. A Comparative Study of Hamilton and Overlap Population Methods for the Analysis of Chemical Bonding. *J. Chem. Phys.* **2000**, *113*, 1698–1704.

(49) Fung, V.; Wu, Z.; Jiang, D.-e. New Bonding Model of Radical Adsorbate on Lattice Oxygen of Perovskites. *J. Phys. Chem. Lett.* **2018**, *9*, 6321–6325.

(50) van Santen, R. A.; Tranca, I.; Hensen, E. J. Theory of Surface Chemistry and Reactivity of Reducible Oxides. *Catal. Today* **2015**, *244*, 63–84.

(51) Yu, L.; Yan, Q.; Ruzsinszky, A. Key Role of Antibonding Electron Transfer in Bonding on Solid Surfaces. *Phys. Rev. Mater.* **2019**, *3*, 092801.

(52) Lin, F.; Wang, S.; Zheng, F.; Zhou, G.; Wu, J.; Gu, B.-L.; Duan, W. Hydrogen-induced Metallicity of SrTiO₃(001) surfaces: A Density Functional Theory Study. *Phys. Rev. B: Condens. Matter Mater. Phys.* **2009**, *79*, 035311.

(53) D'Angelo, M.; Yukawa, R.; Ozawa, K.; Yamamoto, S.; Hirahara, T.; Hasegawa, S.; Silly, M. G.; Sirotti, F.; Matsuda, I. Hydrogen-Induced Surface Metallization of SrTiO₃(001). *Phys. Rev. Lett.* **2012**, *108*, 116802.

(54) Gao, Y.; Huang, R.; Wang, J.; Wu, Z.; Jiang, D.-e. Effect of Hydrogen-Induced Metallization on Chemisorption. *J. Phys. Chem. C* **2019**, *123*, 15171–15175.

(55) Hu, G.; Wu, Z.; Jiang, D.-e. First Principles Insight into H₂ Activation and Hydride Species on TiO₂ Surfaces. *J. Phys. Chem. C* **2018**, *122*, 20323–20328.

(56) Yan, Y.; Shi, W.; Yuan, Z.; He, S.; Li, D.; Meng, Q.; Ji, H.; Chen, C.; Ma, W.; Zhao, J. The Formation of Ti-H Species at Interface Is Lethal to the Efficiency of TiO₂-Based Dye-Sensitized Devices. *J. Am. Chem. Soc.* **2017**, *139*, 2083–2089.

(57) Szilvási, T.; Chen, B. W. J.; Mavrikakis, M. Identification of Stable Adsorption sites and Diffusion Paths on Nanocluster Surfaces: an Automated Scanning Algorithm. *npj Comput. Mater.* **2019**, *5*, 101.

(58) Jäger, M. O. J.; Morooka, E. V.; Federici Canova, F.; Himanen, L.; Foster, A. S. Machine Learning Hydrogen Adsorption on Nanoclusters Through Structural Descriptors. *npj Comput. Mater.* **2018**, *4*, 37.